SUPPORTING INFORMATION

Light-Induced EPR Study of Charge Transport in Fullerene and Non-Fullerene PBDB-T-based Solar Cells

Victor I. Krinichnyi[*†], Evgeniya I. Yudanova[†], Nikolay N. Denisov[†], Aleksei A. Konkin[‡,$], Uwe Ritter[‡], Victor R. Bogatyrenko[†], and Alexander L. Konkin[‡]

[†]Department of Kinetics and Catalysis, Institute of Problems of Chemical Physics RAS, Academician Semenov Avenue 1, 142432 Chernogolovka, Russia

[‡]Center for Micro- and Nanotechnologies, Ilmenau University of Technology, Gustav-Kirchhoff-Str.7, D-98693 Ilmenau, Germany

[$]Institute of Physics, Kazan Federal University, Kremlyovskaya St. 18, 420008 Kazan, Russia

SI-I. NIR-Vis-UV Spectra of the Samples.

Figure S1 depicts the NIR-Vis-UV absorption spectra of the polymer composites studied as well as their initial PBDB-T matrix and PPO layers obtained at T = 298 K by using spectrophotometer Specord-250-plus (Analytik Jena) scanning within the photon energy/wavelength band of 1.13-6.53/1100-190 eV/nm. All the characteristic points of the spectra were determined accurately from their differentiation.

[*] Author to whom any correspondence should be addressed. E-mail: kivirus@gmail.com, Tel.: +7(496-52)21882

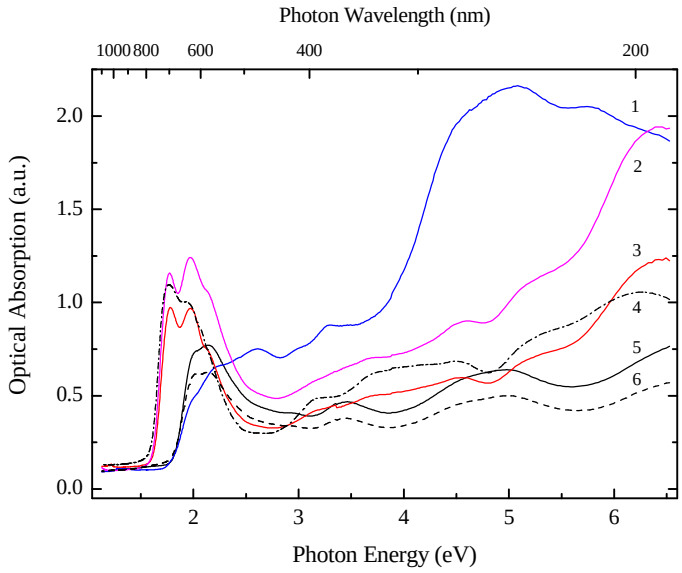

Figure S1. NIR-Vis-UV absorption spectra of the PBDB-T:$PC_{71}BM$ (1), PBDB-T:ITIC-M/$PPO_{0.06}$ (2), PBDB-T:ITIC-M (3), ITIC-M (4), PBDB-T:$PC_{61}BM$ (5) and PBDB-T (6) obtained at T = 298 K.

SI-II. LED Sources Used in Experiments.

Chromatic (with the photon energy/wavelength of 1.34–3.41/923–364 eV/nm) and achromatic white (with the color temperature of T_c = 5000 K) CREE XM-1.2 LED-based light sources were used in experiments for exciting of spin charge carriers in the composites under study.

Figure S2 shows the current-voltage characteristics of some exemplary LEDs, recorded from the value of the luminosity onset current to the maximum value of the LED limiting heating current. The irradiation of the sources was directed through a cylindrical quartz stock in a configuration identical to the LEPR experiments into broadband optical radiometer IMO-2N with a thermocouple-based sensor and where was precision measured. The data presented indicate a symbatic change in the irradiated power of light sources and the forward current passing through them, which is consistent with the fundamental principles of light emission by a semiconductor junction. One can only note a slight difference in these dependencies. The dependence obtained for the white light source contains a pronounced initial induction section (Fig. S2). On the other hand, chromatic light sources with photon energies of 1.47 and 1.90 eV exhibit dependences characteristic of a semiconductor transition (diode waveform)[1] and nearly of resistive system,

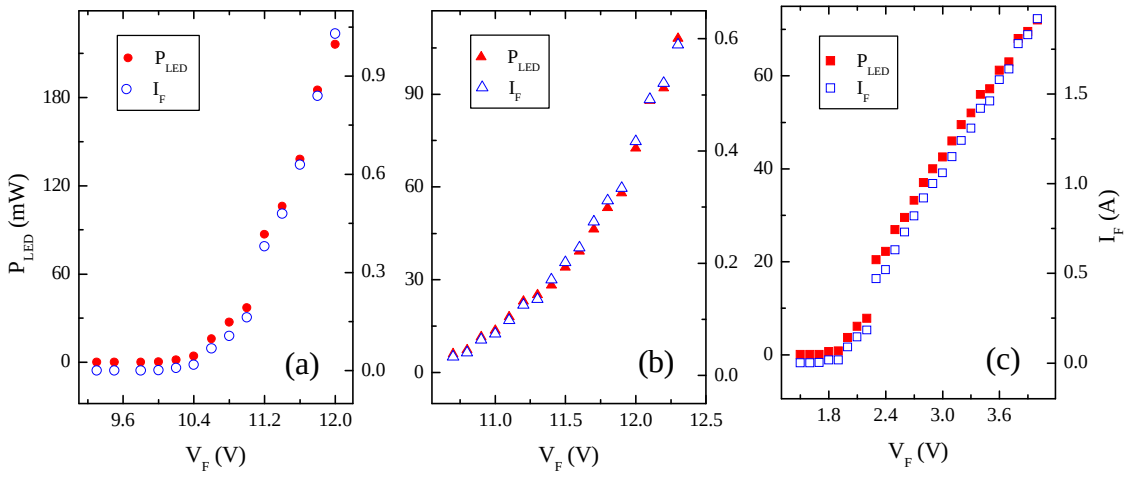

Figure S2. The power P_{LED} illuminated by the achromatic, white light with the color temperature of T_c = 5000 K, (*a*) as well as by the chromatic, with the photon energy/wavelength of 1.47/843 eV/nm (*b*) and 1.90/653 eV/nm (*c*) LED sources as a function of the forward voltage V_F supplied and the current I_F flowing through it at a temperature of T = 300 K.

respectively. This difference in characteristics could be due to the design qualities, e.g., the different number of emitting modules, of these devices.

Another key task was to set the optimal illumination power of the LED-based source that does not saturate the effective LEPR spectra of the samples. This could be realized by establishing maximal illuminance, I_{LED}, on the linear section of such a dependence far enough from the saturation conditions. For this purpose, it was registered LEPR spectra and their resonant contributions due to electron donors and accepters photoexcited in the PBDB-T:$PC_{61}BM$, PBDB-T:$PC_{71}BM$, and PBDB-T:ITIC-M composites upon their steady-state irradiation by the white light source with a color temperature of T_c = 5000 K at variation in its illumination level I_{LED}. Figure S3 shows how changes the concentration n_i of these paramagnetic centers at varying of the I_{LED} value. The analysis of the data presented evidence that this parameter of the total charge carriers as well polarons and radical anions follow the low

$$n_i(I_{LED}) = n_i^0 I_{LED}^{\theta}, \qquad \text{(S1)}$$

where n_i^0 is constant and θ is an exponent depending on the energetic features of photons originating the initial excitons, spin charge carriers, and their microenvironment, including the spin traps capturing them. The θ values obtained from the data presented in Fig. S2 for all

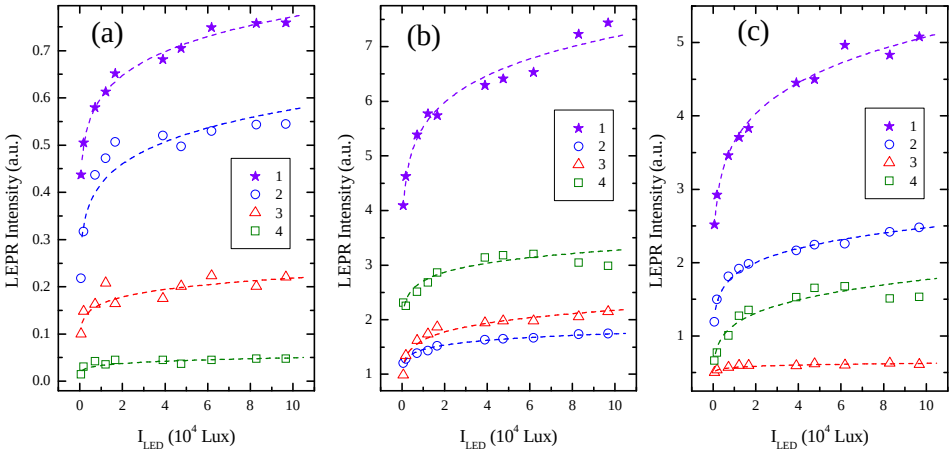

Figure S3. Total spin concentration (*1*) and its contributions due to the polarons PBDB-$T^{+\cdot}_{loc}$ (*2*), mobile and localized counterions $A^{-\bullet}_{mob}$ (*3*) and $A^{-\bullet}_{loc}$ (*4*), respectively, background excited in the PBDB-T:$PC_{61}BM$ (*a*), PBDB-T:$PC_{71}BM$ (*b*), and PBDB-T:ITIC-M (*c*) composites at T = 77 K as a function of the illuminance, I_{LED}, of the achromatic, white light source with the color temperature of T_c = 5000 K. The dependences calculated from Eq.(S1) with θ exponents summarized in the Table S1 are shown by the dashed lines.

charge carriers excited in the samples by photons of white and chromatic light are summarized in Table S1.

Table S1. The Exponent θ in Eq.(S1) Obtained From the Total LEPR Spectra and their Contributions due to the mobile and trapped spin charge carriers excited in the composites' bulk heterojunctions upon their steady-state illumination by the LED with achromatic, white light with the color temperature of T_c = 5000 K (θ_1) as well as by the chromatic LEDs with the photon energy/wavelength of 1.47/843 eV/nm (θ_2) and 1.90/653 eV/nm (θ_3).

Parameters	Sum	$D^{+\cdot}_{loc}$	$D^{+\cdot}_{mob} - A^{-\cdot}_{mob}$	$A^{-\bullet}_{loc}$
	PBDB-T:$PC_{61}BM$			
θ_1	0.109	0.139	0.125	0.171
θ_2	0.059	0.086	0.179	0.248
θ_3	0.606	0.058	0.153	0.137
	PBDB-T:$PC_{71}BM$			
θ_1	0.114	0.079	0.125	0.082
θ_2	0.116	0.121	0.161	0.229
θ_3	0.096	0.119	0.101	0.205
	PBDB-T:ITIC-M			
θ_1	0.143	0.131	0.042	0.186
θ_2	0.119	0.115	0.163	0.072
θ_3	0.094	0.103	0.081	0.075

Now one may evaluate directly from the optical spectra of the samples the number and energy of photons initiating these charge carriers. Figure S4 depicts the normalized optical spectra obtained for the LEDs used in LEPR experiments after optimization their I_{LED} parameter and operation conditions. It is seen from the Figure, that the LEDs demonstrate expectable narrow emission lines whose half-height linewidth variates within the 0.06-0.17 eV region. The spectrum of the white LED source consists of a combination of at least four bands following their color temperature of T_c = 5000 K.[2-3] The energetic parameters of the LEDs used in experiments are summarized in Table S2.

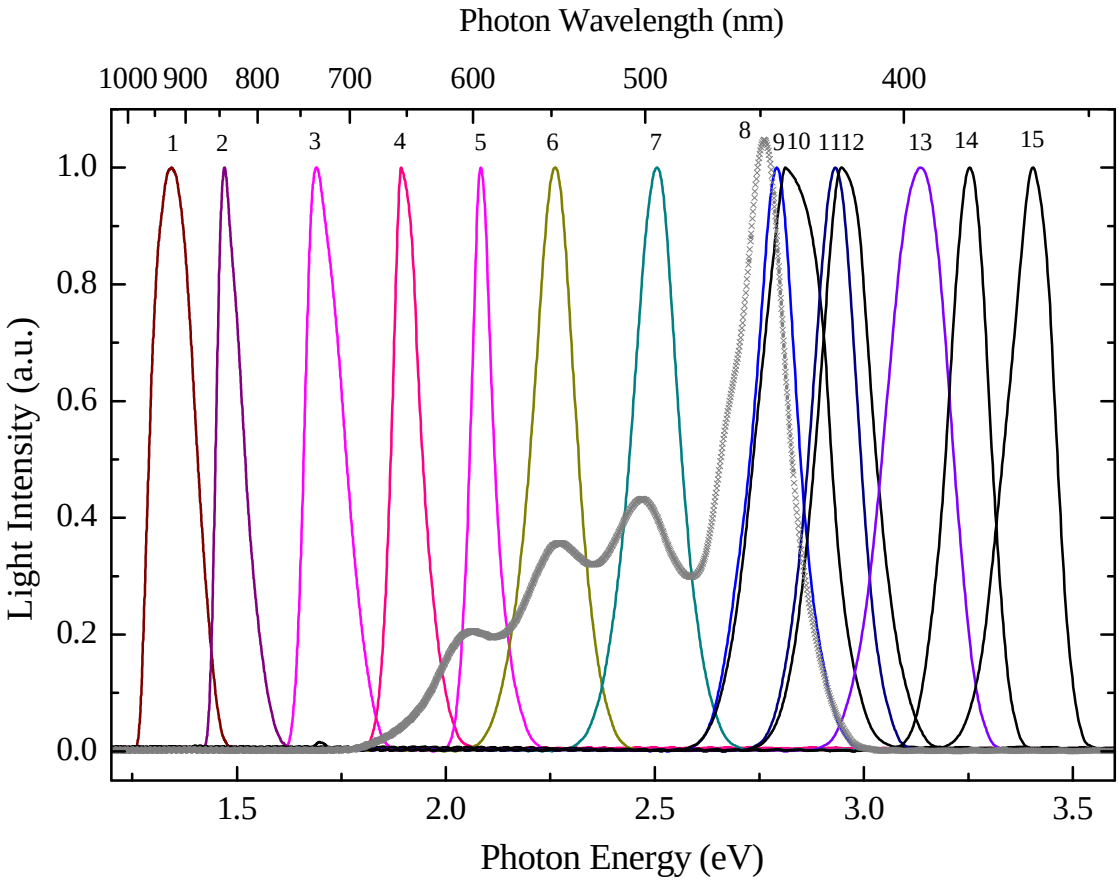

Figure S4. The monochromatic, with the photon energy/wavelength of 1.34/923 (*1*), 1.47/843 (*2*), 1.69/734 (*3*), 1.90/653 (*4*), 2.03/612 (*5*), 2.08/595 (*6*), 2.26/548 (*7*), 2.51/495 (*9*), 2.54/488 (*10*), 2.79/444 (*11*), 2.93/423 (*12*), 3.13/396 (*13*), 3.25/381 (*14*), 3.41/364 (*15*) eV/nm, and achromatic, white, with the color temperature of T_c = 5000 K (*8*) irradiation spectra of the LED sources used in LEPR experiments. The numbering of the spectra is manufactured according to Table S2. The main parameters of the sources are summarized in Table S2.

Table S2. The wavelength, l_{ph}, energy, $h\nu_{ph}$, illuminance, I_{LED}, and irradiation power, P_{LED}, of the chromatic and achromatic [white with the color temperature of T_c = 5000 K (W5K)], LED sources used for steady-state excitation of spin charge carriers in the samples under study.

No	λ_{ph}, nm	$h\nu_{ph}$,eV	I_{LED}, lux	P_{LED}, mW
1	923	1.34	229600	140
2	843	1.47	385400	150
3	734	1.69	188600	115
4	653	1.90	111520	68
5	612	2.03	121360	74
6	595	2.08	49200	30
7	548	2.26	41000	25
8	W5K	W5K	105300	235
9	495	2.51	91840	56
10	488	2.54	90200	55
11	444	2.79	252260	154
12	423	2.93	152520	93
13	396	3.13	141040	86
14	381	3.25	205000	125
15	364	3.41	96760	59

SI-III. Spin-Lattice Relaxation of Charge Carriers in PBDB-Based Composites.

Figure S5 demonstrates the change of amplitudes of effective LEPR spectra of the samples illuminated by white light with the color temperature of 5000 K at T_c = 77 K as well as their spectral contributions due to mobile and localized spin charge carriers with a magnetic term B_1 of MW field in the spectrometer's resonator. The nonlinear behavior of these dependences indicates an appearance of MW saturation of all paramagnetic centers, which is determined by their electron relaxation which is described by the spin-lattice and spin-spin relaxation times, T_1 and T_2, respectively. In this case, the dependencies should be described by the following equation[4-5]

$$I = I_0 B_1 (1 + \gamma_e^2 B_1^2 T_1 T_2)^{-3/2}, \quad \text{(S2)}$$

where I_0 is the initial amplitude of signal far from MW saturation, B_1 is the value of a magnetic term of MW field, and γ_e is the gyromagnetic ratio for electron. The dependences calculated from Eq.(S2) with the data presented in Table S3 are seen in the Figure to be fitted well all the experimental data.

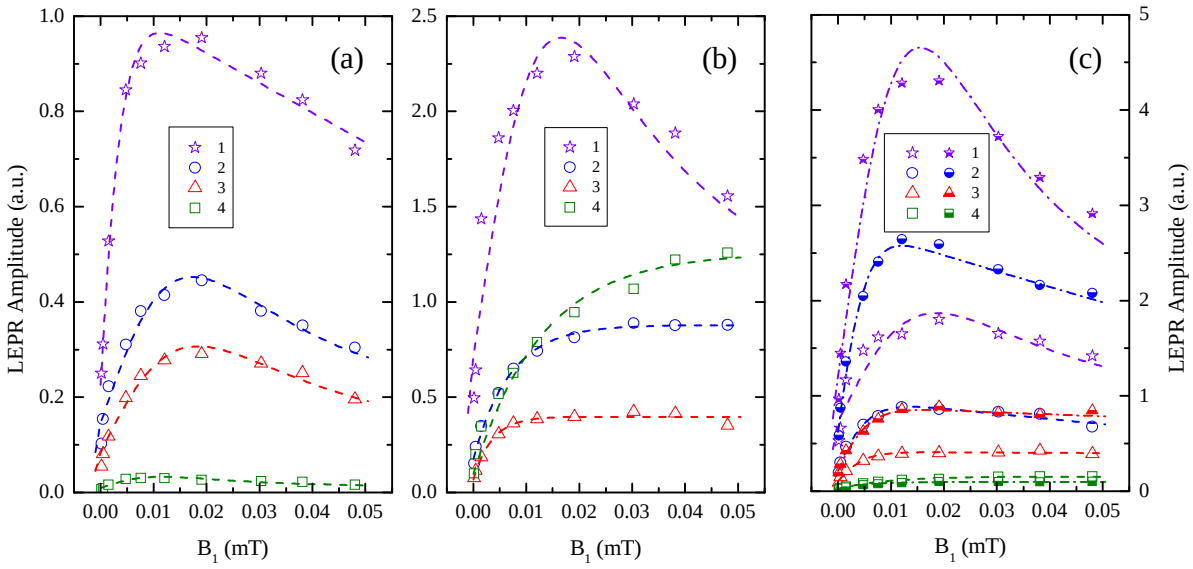

Figure S5. Relative effective amplitudes (1) of spin charge carriers and its contributions due to the polarons PBDB-$T^{+\cdot}_{loc}$ (*2*), mobile and localized counterions $A^{-\bullet}_{mob}$ (*3*) and $A^{-\bullet}_{loc}$ (*4*), respectively, background excited in the PBDB-T:$PC_{61}BM$ (*a*), PBDB-T:$PC_{71}BM$ (*b*), PBDB-T:ITIC-M, and PBDB-T:ITIC-M/$PPO_{0.06}$ (*c*) composites by an achromatic, white light source with the color temperature T_c = 5000 K at T = 77 K, as a function of magnetic term B_1 of MW field. The lines calculated from Eq.(S2) with the data presented in Table S3 are shown as well.

Table S3. The spin-lattice T_1 and spin-spin T_2 relaxation times of the mobile and trapped spin charge carriers excited in the donor-acceptor composites upon their steady-state illumination by the LED source of achromatic, white light with the color temperature of T_c = 5000 K.

Parameter	$D^{+\cdot}_{loc}$	$D^{+\cdot}_{mob} - A^{-\cdot}_{mob}$	$A^{-\bullet}_{loc}$
	PBDB-T:$PC_{61}BM$		
T_1, s	1.48×10^{-6}	1.44×10^{-6}	1.40×10^{-6}
T_2, s	5.04×10^{-8}	6.90×10^{-8}	6.83×10^{-8}
	PBDB-T:$PC_{71}BM$		
T_1, s	5.73×10^{-7}	8.18×10^{-7}	7.25×10^{-8}
T_2, s	5.12×10^{-8}	3.86×10^{-8}	3.81×10^{-8}
	PBDB-T:ITIC-M		
T_1, s	1.35×10^{-6}	5.57×10^{-7}	3.64×10^{-7}
T_2, s	4.07×10^{-8}	5.46×10^{-8}	5.38×10^{-8}
	PBDB-T:ITIC-M/$PPO_{0.06}$		
T_1, s	1.32×10^{-6}	4.50×10^{-7}	2.73×10^{-7}
T_2, s	4.05×10^{-8}	6.83×10^{-8}	6.77×10^{-8}

SI-IV. Structure and HFC Parameters ($A_{iso}=A_0$) of Monomer 1-BDB-T

[Calculations in SI-IV and SI-V were performed in G16 (6)]

SI-IVa. 1-BDB-T monomer structure.

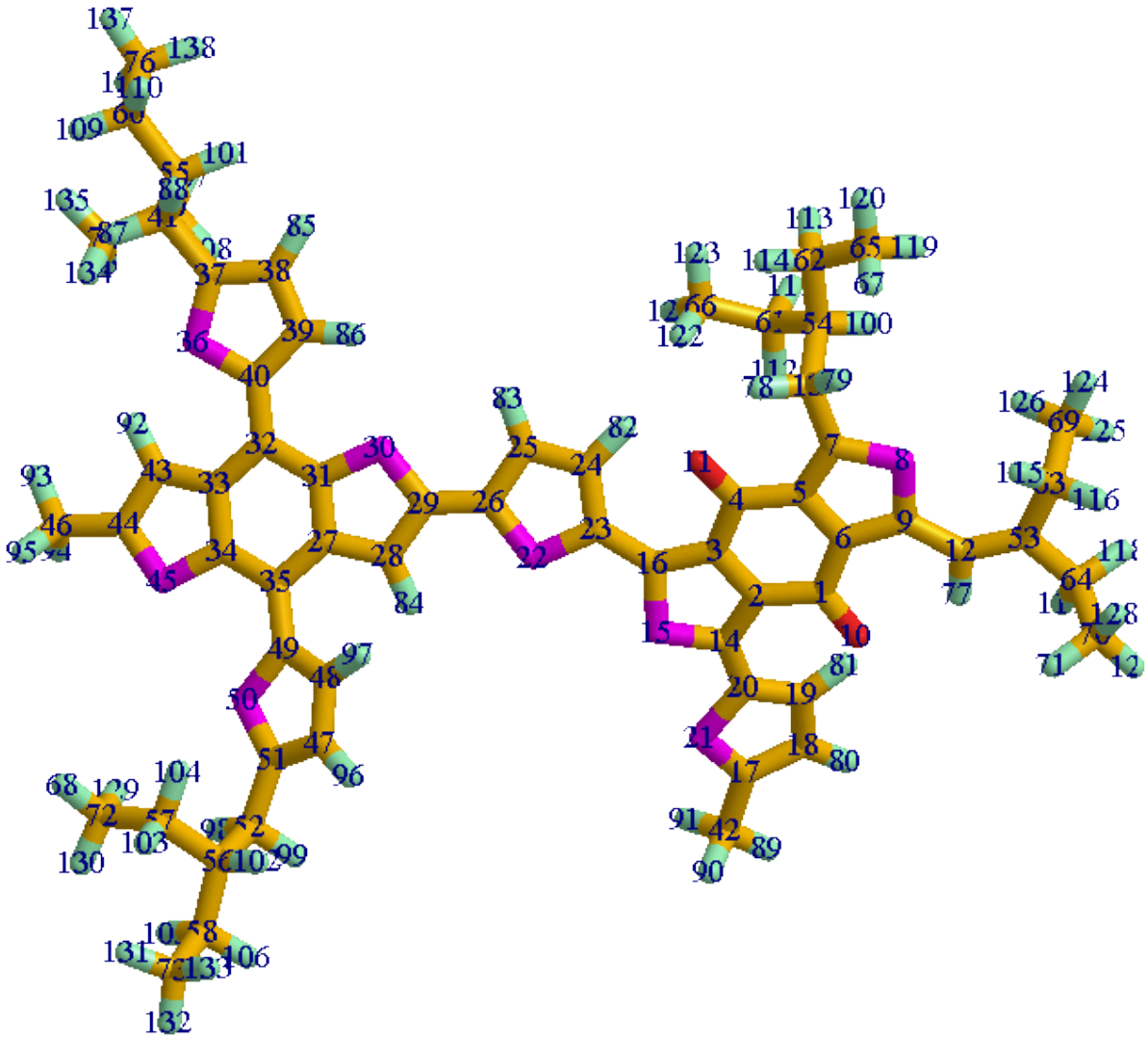

Table S4. ^1H isotropic Fermi contact couplings A_{iso} (in G/0.1 mT) of the 1-BDB-T monomer.

N atom	Gauss	N atom	Gauss
67	0,00127	108	0,00377
68	0,00493	109	-0,01242
71	-0,0067	110	-0,01497
75	0,00492	111	3,4E-4
77	-0,00352	112	4E-4
78	0,06497	113	0,01368
79	0,00764	114	5E-4
80	0,04548	115	0,04186
81	-0,40407	116	0,04798
82	-0,63451	117	0,03757
83	-0,10135	118	0,05803
84	-4,13597	119	-1,3E-4
85	-0,08628	120	5,7E-4
86	-1,09274	121	-0,00192
87	0,16138	122	0,00215
88	1,95695	123	-0,00184
89	0,03376	124	0,01771
90	1,24192	125	-0,00697
91	1,1513	126	-0,00679
92	-1,92394	127	0,02592
93	-0,01891	128	-0,00663
94	1,21949	129	-0,00422
95	1,10815	130	0,03911
96	0,41534	131	-4,8E-4
97	-1,81314	132	0,12956
98	0,22647	133	7,4E-4
99	2,88103	134	-0,00291
100	-0,00301	135	0,02665
101	-0,1095	136	-0,00104
102	-0,17479	137	0,0948
103	0,0291	138	0,00146

SI-IVb. 4-BDB-T oligomer structure.

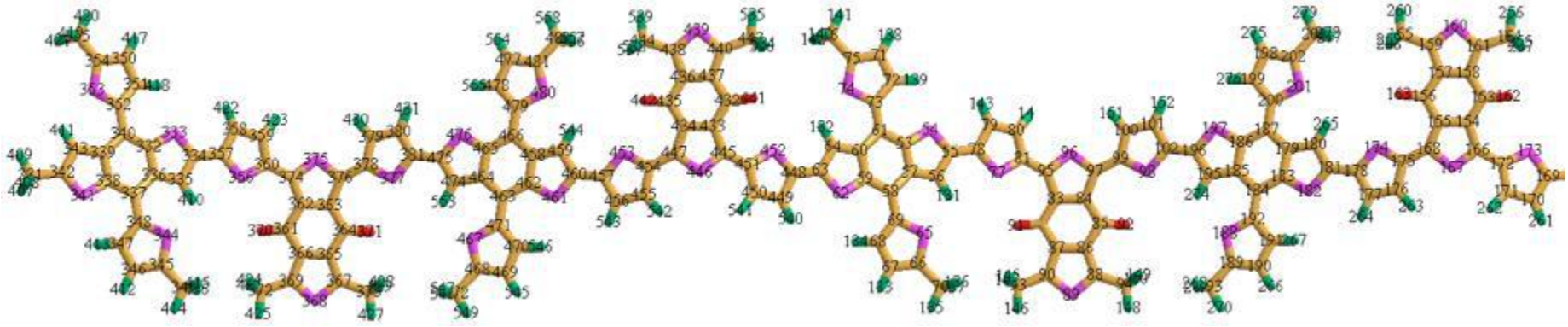

Table S5. ^{1}H Isotropic Fermi contact couplings, A_{iso} (in Gauss/0.1 mT) of the 4-BDB-T oligomer.

N atom	Gauss	N atom	Gauss	N atom	Gauss	N atom	Gauss
51	-0,72235	124	0,0042	200	0,25448	275	0,00952
52	-0,70418	125	-2,8E-4	201	0,23111	276	-7,6E-4
53	0,00318	126	0,00195	202	-0,01163	277	0,00472
54	-0,33531	127	5,5E-4	203	-1,02173	278	0,00374
55	0,02276	128	0,00401	204	-0,68375	279	0,00965
56	0,73341	129	-3,4E-4	205	0,00985	280	-7,3E-4
57	0,71	130	-0,00288	206	-0,4922	281	-0,04347
58	0,00353	131	-0,01053	207	0,03594	282	-0,07215
59	-0,33965	132	-0,0889	208	1,10007	283	-0,07521
60	0,73691	133	-0,03994	209	1,02685	284	-0,04431
61	0,02235	134	-1,04157	210	4E-5	285	-0,73904
62	0,72663	135	0,00965	211	-0,39664	286	0,00216
63	-0,04599	136	-0,50443	212	0,93011	287	-0,35116
64	-0,07798	137	1,10168	213	0,02803	288	0,77598
65	0,00429	138	1,05142	214	0,88189	289	0,74379
66	-8,5E-4	139	0,03429	215	-0,02564	290	0,02409
67	0,01084	140	7,5E-4	216	-0,09409	291	-0,74819
68	-9,1E-4	141	0,03101	217	0,00201	292	0,00606
69	0,0039	142	0,03013	218	-6,9E-4	293	-0,35289
70	0,01175	143	-1,0233	219	0,00742	294	0,77798
71	-0,09683	144	0,00139	220	-8E-4	295	0,73997
72	-0,0526	145	-0,48923	221	0,00349	296	0,02441
		146	1,10657	222	0,00942		
		147	1,05139	223	-0,07715		
		148	0,03399	224	-0,04424		

SI-V. Structure and HFC Parameters ($A_{iso}=A_0$) of Single 1-ITIC-pl and Double 2-ITIC-pl.

SI-Va. 1-ITIC-pl.

Table S6. ^{1}H Isotropic Fermi contact couplings, A_{iso} (in Gauss/0.1 mT) of the 1-ITIC-pl.

Atom	a.u.	MegaHertz	Gauss	10(-4) cm-1
82 H(1)	-0.00074	-3.28567	-1.17241	-1.09598
83 H(1)	0.00011	0.49283	0.17586	0.16439
84 H(1)	-0.00068	-3.05137	-1.08880	-1.01783
85 H(1)	-0.00275	-12.28198	-4.38251	-4.09683
86 H(1)	-0.00125	-5.58293	-1.99213	-1.86226
87 H(1)	0.00001	0.04586	0.01636	0.01530
88 H(1)	0.00000	0.00092	0.00033	0.00031
89 H(1)	0.00000	0.01463	0.00522	0.00488
90 H(1)	-0.00000	-0.02188	-0.00781	-0.00730
91 H(1)	-0.00001	-0.03288	-0.01173	-0.01097
92 H(1)	0.00000	0.01347	0.00481	0.00449
93 H(1)	-0.00000	-0.00233	-0.00083	-0.00078
94 H(1)	-0.00000	-0.00915	-0.00326	-0.00305
95 H(1)	-0.00022	-0.97389	-0.34751	-0.32486
96 H(1)	-0.00022	-0.97830	-0.34908	-0.32633
97 H(1)	-0.00000	-0.00943	-0.00336	-0.00314
98 H(1)	-0.00000	-0.00162	-0.00058	-0.00054
99 H(1)	0.00000	0.01416	0.00505	0.00472
100 H(1)	-0.00001	-0.03239	-0.01156	-0.01080
101 H(1)	-0.00000	-0.02212	-0.00789	-0.00738
102 H(1)	0.00000	0.01462	0.00522	0.00488
103 H(1)	0.00000	0.00079	0.00028	0.00026
104 H(1)	0.00001	0.04667	0.01665	0.01557
105 H(1)	-0.00125	-5.59850	-1.99768	-1.86746
106 H(1)	-0.00275	-12.31051	-4.39270	-4.10634
107 H(1)	0.00011	0.49399	0.17627	0.16478
108 H(1)	-0.00068	-3.05841	-1.09132	-1.02018
110 H(1)	-0.00074	-3.29314	-1.17508	-1.09847
115 H(1)	-0.00000	-0.00081	-0.00029	-0.00027
116 H(1)	-0.00000	-0.00116	-0.00041	-0.00039
117 H(1)	-0.00000	-0.01226	-0.00438	-0.00409
118 H(1)	-0.00000	-0.01218	-0.00435	-0.00406
119 H(1)	-0.00000	-0.00128	-0.00046	-0.00043
120 H(1)	-0.00000	-0.00062	-0.00022	-0.00021
121 H(1)	0.00000	0.00033	0.00012	0.00011
122 H(1)	0.00000	0.01316	0.00470	0.00439
123 H(1)	0.00000	0.00481	0.00172	0.00160
124 H(1)	0.00000	0.00996	0.00355	0.00332
125 H(1)	0.00000	0.00357	0.00127	0.00119
126 H(1)	0.00000	0.00175	0.00062	0.00058
127 H(1)	-0.00023	-1.01164	-0.36098	-0.33745
128 H(1)	-0.00022	-0.99370	-0.35458	-0.33146
129 H(1)	-0.00004	-0.15830	-0.05648	-0.05280
130 H(1)	-0.00023	-1.01322	-0.36154	-0.33797
131 H(1)	-0.00004	-0.15855	-0.05658	-0.05289
132 H(1)	-0.00022	-0.99580	-0.35533	-0.33216

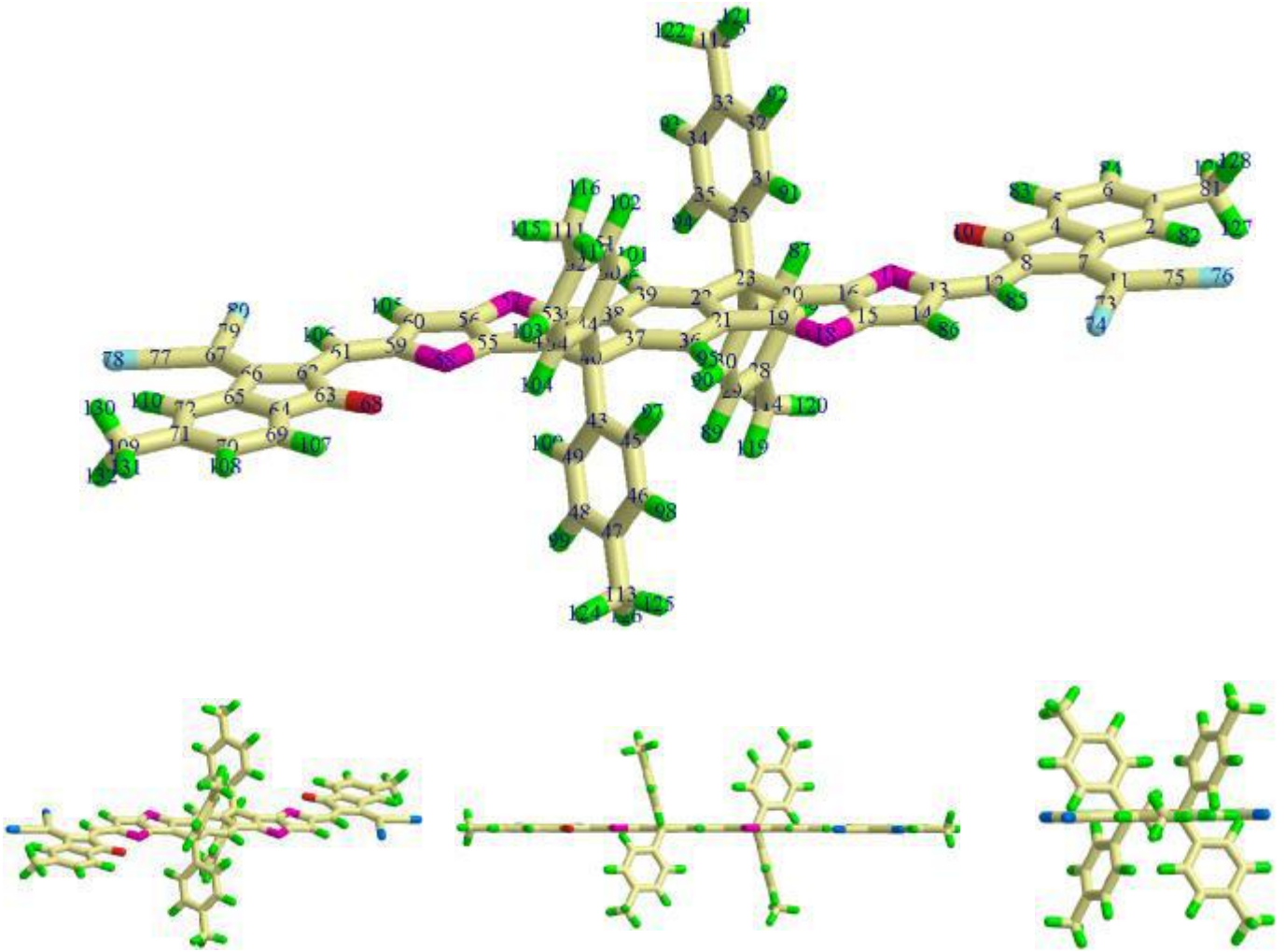

Figure S6. ITIC-pl with the atom numbered (above) in case of different orientations/projections (below).

SI-Vb. 2-ITIC-pl: ^{1}H isotropic Fermi Contact Couplings A_{iso}.

Table S7. ^{1}H Isotropic Fermi contact couplings, A_{iso} (in Gauss/0.1 mT) of the 2-ITIC-pl.

Atom	a.u.	MegaHertz	Gauss	10(-4) cm^{-1}
82 H(1)	-0.00032	-1.45091	-0.51772	-0.48397
83 H(1)	0.00003	0.14845	0.05297	0.04952
84 H(1)	-0.00031	-1.39327	-0.49715	-0.46474
85 H(1)	-0.00120	-5.36229	-1.91340	-1.78867
86 H(1)	-0.00055	-2.43862	-0.87016	-0.81344
87 H(1)	0.00000	0.01806	0.00645	0.00603
88 H(1)	0.00000	0.00217	0.00077	0.00072
89 H(1)	0.00000	0.00871	0.00311	0.00291
90 H(1)	-0.00000	-0.01080	-0.00385	-0.00360
91 H(1)	-0.00000	-0.00098	-0.00035	-0.00033
92 H(1)	-0.00000	-0.00557	-0.00199	-0.00186
93 H(1)	-0.00000	-0.00021	-0.00007	-0.00007
94 H(1)	-0.00000	-0.00456	-0.00163	-0.00152
95 H(1)	-0.00009	-0.39100	-0.13952	-0.13042
96 H(1)	-0.00013	-0.58301	-0.20803	-0.19447
97 H(1)	-0.00000	-0.00686	-0.00245	-0.00229
98 H(1)	-0.00000	-0.00133	-0.00048	-0.00044
99 H(1)	0.00000	0.00577	0.00206	0.00192
100 H(1)	-0.00000	-0.01485	-0.00530	-0.00495
101 H(1)	-0.00000	-0.00988	-0.00353	-0.00330
102 H(1)	0.00000	0.00715	0.00255	0.00238
103 H(1)	0.00000	0.00033	0.00012	0.00011
104 H(1)	0.00001	0.02258	0.00806	0.00753
105 H(1)	-0.00074	-3.30155	-1.17808	-1.10128
106 H(1)	-0.00160	-7.17382	-2.55980	-2.39293
107 H(1)	0.00008	0.35585	0.12698	0.11870
229 H(1)	-0.00000	-0.00454	-0.00162	-0.00152
230 H(1)	-0.00000	-0.00001	-0.00000	-0.00000
231 H(1)	-0.00000	-0.00542	-0.00193	-0.00181
232 H(1)	-0.00000	-0.00097	-0.00035	-0.00032
233 H(1)	-0.00000	-0.01077	-0.00384	-0.00359
234 H(1)	0.00000	0.00871	0.00311	0.00291
235 H(1)	0.00000	0.00220	0.00078	0.00073
236 H(1)	0.00000	0.01802	0.00643	0.00601
237 H(1)	-0.00054	-2.43583	-0.86917	-0.81251
238 H(1)	-0.00120	-5.35798	-1.91186	-1.78723
239 H(1)	0.00003	0.14810	0.05285	0.04940
240 H(1)	-0.00031	-1.39170	-0.49659	-0.46422
242 H(1)	-0.00032	-1.44913	-0.51709	-0.48338
247 H(1)	0.00000	0.00157	0.00056	0.00052
248 H(1)	-0.00000	-0.00082	-0.00029	-0.00028
249 H(1)	-0.00000	-0.00342	-0.00122	-0.00114
250 H(1)	-0.00000	-0.00873	-0.00311	-0.00291
108 H(1)	-0.00042	-1.85699	-0.66262	-0.61943
110 H(1)	-0.00044	-1.98102	-0.70688	-0.66080
115 H(1)	-0.00000	-0.00170	-0.00061	-0.00057
116 H(1)	-0.00000	-0.00102	-0.00036	-0.00034
117 H(1)	-0.00000	-0.00874	-0.00312	-0.00292
118 H(1)	-0.00000	-0.00342	-0.00122	-0.00114
119 H(1)	-0.00000	-0.00083	-0.00030	-0.00028
120 H(1)	0.00000	0.00158	0.00056	0.00053
121 H(1)	0.00000	0.00315	0.00112	0.00105
122 H(1)	0.00000	0.00260	0.00093	0.00087
123 H(1)	-0.00000	-0.00044	-0.00016	-0.00015
124 H(1)	0.00000	0.00626	0.00223	0.00209
125 H(1)	0.00000	0.00098	0.00035	0.00033
126 H(1)	0.00000	0.00240	0.00086	0.00080
127 H(1)	-0.00012	-0.55520	-0.19811	-0.18519
128 H(1)	-0.00009	-0.39670	-0.14155	-0.13233
129 H(1)	-0.00002	-0.07657	-0.02732	-0.02554
130 H(1)	-0.00015	-0.65278	-0.23293	-0.21775
131 H(1)	-0.00002	-0.09765	-0.03484	-0.03257
132 H(1)	-0.00015	-0.66954	-0.23891	-0.22333
214 H(1)	-0.00044	-1.97243	-0.70381	-0.65793
215 H(1)	0.00008	0.35413	0.12636	0.11812
216 H(1)	-0.00041	-1.84929	-0.65987	-0.61686
217 H(1)	-0.00160	-7.14711	-2.55027	-2.38402
218 H(1)	-0.00074	-3.28801	-1.17325	-1.09676
219 H(1)	0.00000	0.02231	0.00796	0.00744
220 H(1)	0.00000	0.00037	0.00013	0.00012
221 H(1)	0.00000	0.00713	0.00254	0.00238
222 H(1)	-0.00000	-0.00985	-0.00352	-0.00329
223 H(1)	-0.00000	-0.01518	-0.00542	-0.00506
224 H(1)	0.00000	0.00532	0.00190	0.00177
225 H(1)	-0.00000	-0.00180	-0.00064	-0.00060
226 H(1)	-0.00000	-0.00662	-0.00236	-0.00221
227 H(1)	-0.00013	-0.58071	-0.20721	-0.19370
228 H(1)	-0.00009	-0.39068	-0.13940	-0.13032
251 H(1)	-0.00000	-0.00102	-0.00036	-0.00034
252 H(1)	-0.00000	-0.00170	-0.00061	-0.00057
253 H(1)	0.00000	0.00142	0.00051	0.00047
254 H(1)	0.00000	0.00849	0.00303	0.00283
255 H(1)	0.00000	0.00156	0.00056	0.00052
256 H(1)	0.00000	0.00349	0.00125	0.00116
257 H(1)	-0.00000	-0.00000	-0.00000	-0.00000
258 H(1)	0.00000	0.00143	0.00051	0.00048
259 H(1)	-0.00015	-0.65002	-0.23194	-0.21682
260 H(1)	-0.00015	-0.66669	-0.23789	-0.22238
261 H(1)	-0.00002	-0.09726	-0.03470	-0.03244
262 H(1)	-0.00012	-0.55483	-0.19798	-0.18507
263 H(1)	-0.00002	-0.07665	-0.02735	-0.02557
264 H(1)	-0.00009	-0.39606	-0.14132	-0.13211

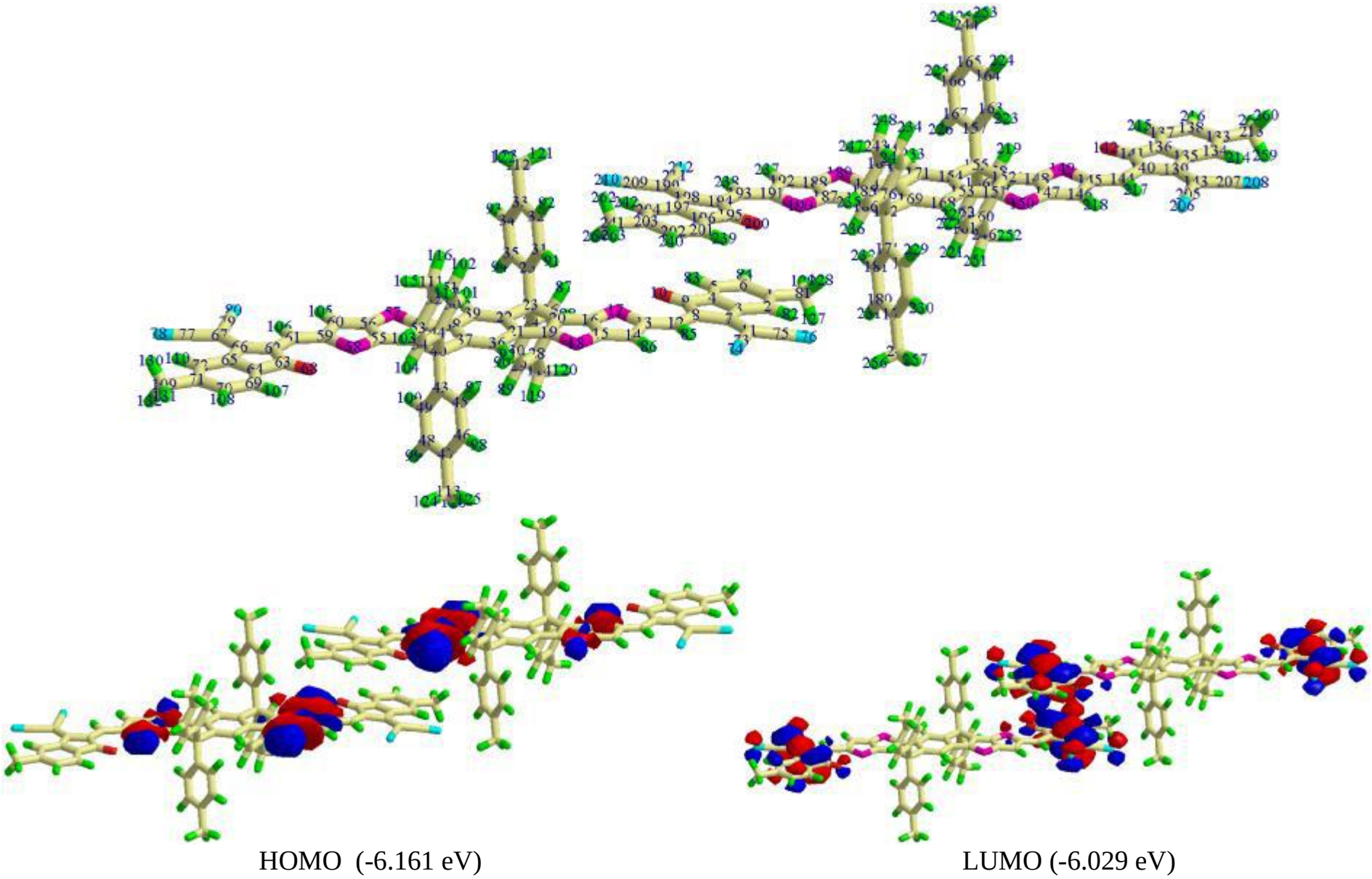

Figure S7. The atoms numbering (above) and HOMO and LUMO energy levels (below) of the 2-ITIC-pl structure.

SI-Vc. 1-ITIC-S-Isomer.

Table S8. ^{1}H Isotropic Fermi contact couplings, A_{iso} (in Gauss/0.1 mT) of the 1-ITIC-S-isomer.

Atom		a.u.	MegaHertz	Gauss	10(-4) cm-1
86	H(1)	-0.00000	-0.01952	-0.00697	-0.00651
87	H(1)	-0.00001	-0.05242	-0.01870	-0.01749
88	H(1)	-0.00001	-0.02884	-0.01029	-0.00962
89	H(1)	-0.00034	-1.50989	-0.53877	-0.50365
90	H(1)	-0.00001	-0.03325	-0.01186	-0.01109
91	H(1)	-0.00033	-1.48071	-0.52836	-0.49391
92	H(1)	-0.00189	-8.43443	-3.00961	-2.81342
93	H(1)	-0.00046	-2.04745	-0.73058	-0.68295
94	H(1)	0.00001	0.05435	0.01939	0.01813
95	H(1)	-0.00001	-0.04800	-0.01713	-0.01601
96	H(1)	-0.00001	-0.05497	-0.01961	-0.01834
97	H(1)	0.00002	0.09428	0.03364	0.03145
98	H(1)	-0.00003	-0.11872	-0.04236	-0.03960
99	H(1)	-0.00001	-0.04658	-0.01662	-0.01554
100	H(1)	0.00001	0.05255	0.01875	0.01753
101	H(1)	-0.00002	-0.08123	-0.02898	-0.02709
102	H(1)	-0.00008	-0.33714	-0.12030	-0.11246
103	H(1)	-0.00006	-0.25650	-0.09152	-0.08556
104	H(1)	-0.00002	-0.07507	-0.02679	-0.02504
105	H(1)	0.00001	0.05537	0.01976	0.01847
106	H(1)	-0.00001	-0.05345	-0.01907	-0.01783
107	H(1)	-0.00003	-0.11573	-0.04130	-0.03860
108	H(1)	0.00002	0.09241	0.03298	0.03083
109	H(1)	-0.00001	-0.05040	-0.01799	-0.01681
110	H(1)	-0.00001	-0.04451	-0.01588	-0.01485
111	H(1)	0.00001	0.05173	0.01846	0.01726
112	H(1)	-0.00044	-1.96848	-0.70240	-0.65661
113	H(1)	-0.00190	-8.49122	-3.02988	-2.83237
114	H(1)	-0.00000	-0.01879	-0.00671	-0.00627
115	H(1)	-0.00034	-1.53380	-0.54730	-0.51162
116	H(1)	-0.00035	-1.56834	-0.55962	-0.52314
117	H(1)	-0.00000	-0.00893	-0.00319	-0.00298
118	H(1)	-0.00004	-0.16367	-0.05840	-0.05460
119	H(1)	-0.00003	-0.14325	-0.05112	-0.04778
120	H(1)	0.00006	0.26600	0.09492	0.08873
121	H(1)	0.00001	0.03241	0.01156	0.01081
122	H(1)	0.00002	0.08487	0.03028	0.02831
123	H(1)	0.00002	0.08309	0.02965	0.02772
124	H(1)	0.00001	0.02938	0.01048	0.00980
125	H(1)	0.00006	0.25122	0.08964	0.08380
126	H(1)	-0.00005	-0.20414	-0.07284	-0.06809
127	H(1)	-0.00002	-0.10103	-0.03605	-0.03370
128	H(1)	-0.00000	-0.02111	-0.00753	-0.00704
129	H(1)	-0.00001	-0.06077	-0.02168	-0.02027
131	H(1)	-0.00001	-0.05600	-0.01998	-0.01868
132	H(1)	-0.00001	-0.04923	-0.01757	-0.01642

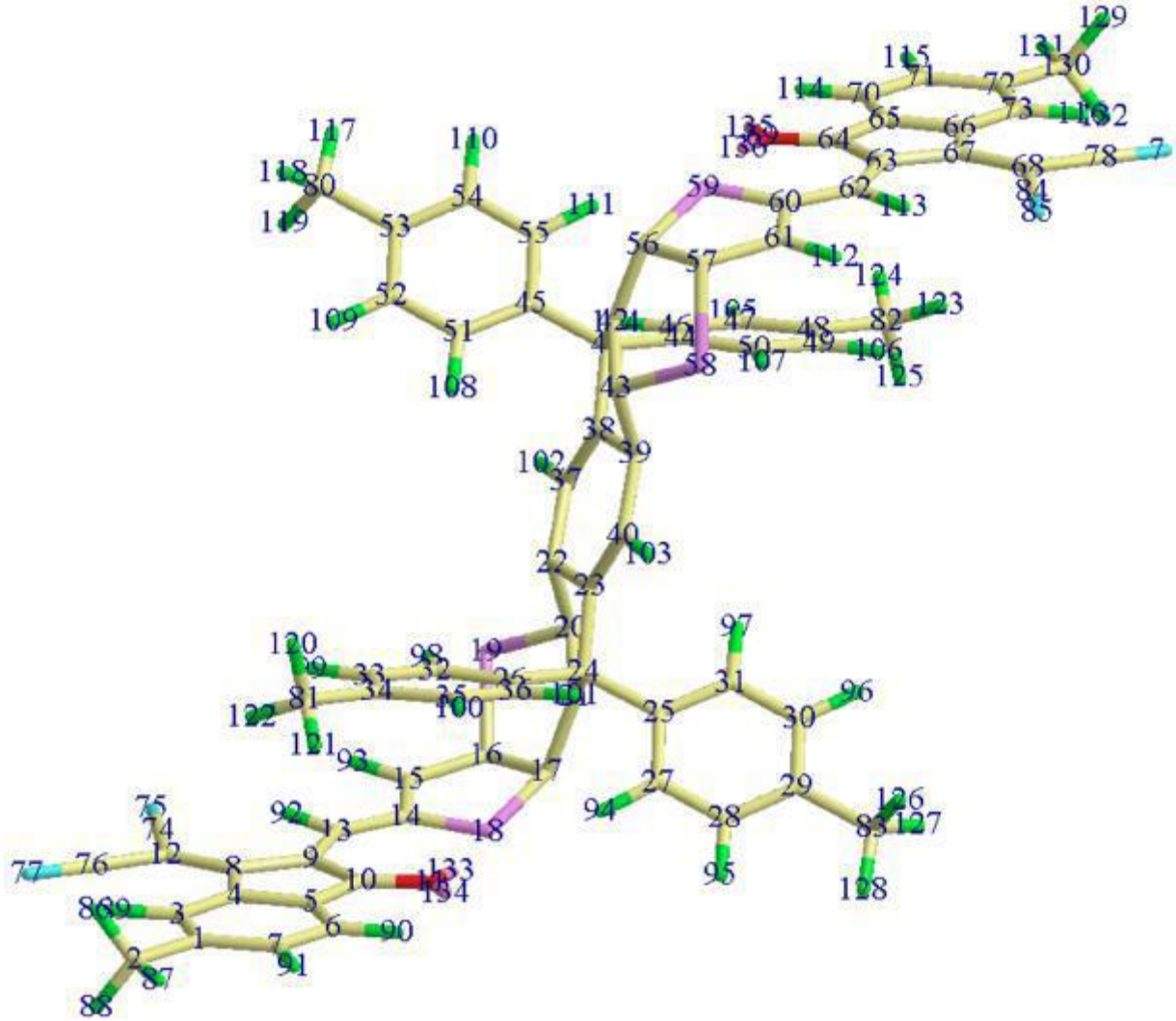

Figure S8. ITIC-S-isomer: all atoms numbering.

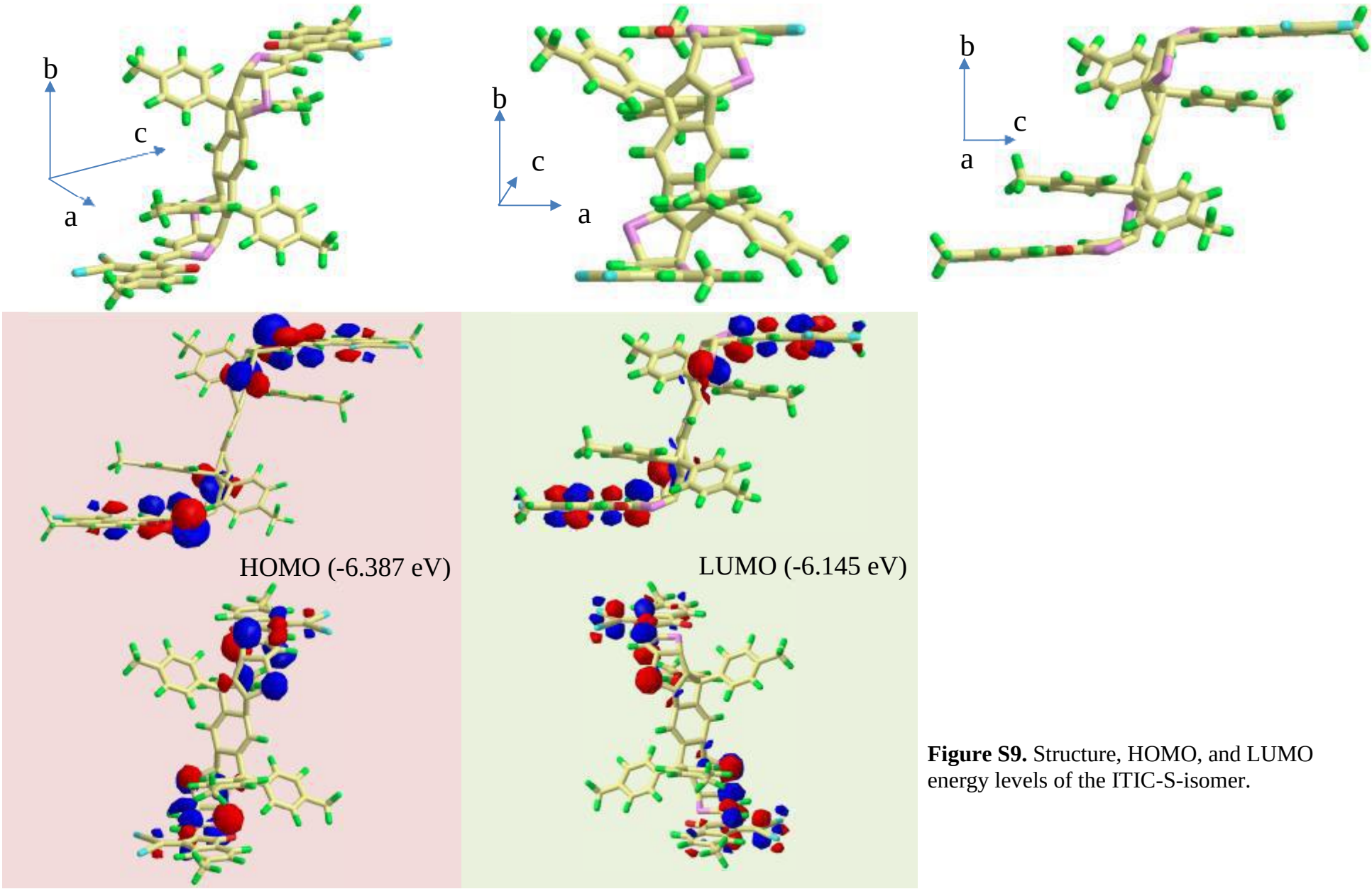

Figure S9. Structure, HOMO, and LUMO energy levels of the ITIC-S-isomer.

SI-Vd. Isotropic Fermi contact couplings of the 2-ITIC-S-isomer.

Table S9. ^{1}H Isotropic Fermi contact couplings, A_{iso} (in Gauss/0.1 mT) of the 2-ITIC-S-isomer.

Atom	a.u.	MegaHertz	Gauss	10^{-4} cm^{-1}
86 H(1)	-0.00003	-0.13784	-0.04918	-0.04598
87 H(1)	-0.00001	-0.03744	-0.01336	-0.01249
88 H(1)	-0.00003	-0.13444	-0.04797	-0.04484
89 H(1)	-0.00022	-0.98591	-0.35180	-0.32886
90 H(1)	0.00000	0.01434	0.00512	0.00478
91 H(1)	-0.00020	-0.90817	-0.32406	-0.30293
92 H(1)	-0.00116	-5.17934	-1.84812	-1.72764
93 H(1)	-0.00057	-2.55994	-0.91345	-0.85390
94 H(1)	0.00002	0.10837	0.03867	0.03615
95 H(1)	-0.00002	-0.06888	-0.02458	-0.02298
96 H(1)	-0.00002	-0.07388	-0.02636	-0.02464
97 H(1)	0.00002	0.08674	0.03095	0.02893
98 H(1)	-0.00004	-0.17107	-0.06104	-0.05706
99 H(1)	-0.00001	-0.02817	-0.01005	-0.00940
100 H(1)	0.00001	0.05540	0.01977	0.01848
101 H(1)	-0.00004	-0.15923	-0.05682	-0.05311
102 H(1)	-0.00040	-1.79280	-0.63971	-0.59801
103 H(1)	0.00031	1.36387	0.48666	0.45494
104 H(1)	0.00001	0.05608	0.02001	0.01871
105 H(1)	0.00000	0.00688	0.00246	0.00230
106 H(1)	-0.00000	-0.01386	-0.00495	-0.00462
107 H(1)	0.00002	0.09025	0.03220	0.03010
108 H(1)	0.00001	0.02947	0.01052	0.00983
109 H(1)	0.00000	0.01040	0.00371	0.00347
110 H(1)	0.00000	0.01699	0.00606	0.00567
111 H(1)	-0.00001	-0.04846	-0.01729	-0.01616
112 H(1)	0.00001	0.02678	0.00955	0.00893
113 H(1)	-0.00063	-2.83758	-1.01252	-0.94651
114 H(1)	0.00001	0.03890	0.01388	0.01298
115 H(1)	-0.00011	-0.47693	-0.17018	-0.15909
116 H(1)	-0.00011	-0.50993	-0.18195	-0.17009
117 H(1)	0.00000	0.00785	0.00280	0.00262
118 H(1)	0.00002	0.08276	0.02953	0.02761
119 H(1)	0.00002	0.07690	0.02744	0.02565
120 H(1)	0.00004	0.19930	0.07111	0.06648
121 H(1)	0.00001	0.03408	0.01216	0.01137
122 H(1)	0.00001	0.05567	0.01986	0.01857
123 H(1)	0.00000	0.02231	0.00796	0.00744
124 H(1)	0.00000	0.00215	0.00077	0.00072
125 H(1)	0.00001	0.04764	0.01700	0.01589
126 H(1)	-0.00007	-0.29371	-0.10480	-0.09797
127 H(1)	-0.00003	-0.14569	-0.05198	-0.04860
128 H(1)	-0.00001	-0.03292	-0.01175	-0.01098
129 H(1)	0.00000	0.00074	0.00027	0.00025
131 H(1)	-0.00000	-0.01786	-0.00637	-0.00596
132 H(1)	0.00000	0.00082	0.00029	0.00027
218 H(1)	0.00003	0.13990	0.04992	0.04666
219 H(1)	-0.00000	-0.00893	-0.00319	-0.00298
220 H(1)	0.00003	0.14965	0.05340	0.04992
221 H(1)	-0.00008	-0.33779	-0.12053	-0.11268
222 H(1)	0.00001	0.05069	0.01809	0.01691
223 H(1)	-0.00010	-0.43098	-0.15378	-0.14376
224 H(1)	-0.00049	-2.17575	-0.77636	-0.72575
225 H(1)	0.00041	1.85012	0.66017	0.61713
226 H(1)	-0.00004	-0.17524	-0.06253	-0.05845
227 H(1)	0.00002	0.07351	0.02623	0.02452
228 H(1)	0.00002	0.07264	0.02592	0.02423
229 H(1)	-0.00000	-0.00976	-0.00348	-0.00326
230 H(1)	0.00007	0.31114	0.11102	0.10379
231 H(1)	-0.00000	-0.00949	-0.00339	-0.00316
232 H(1)	-0.00001	-0.04004	-0.01429	-0.01336
233 H(1)	0.00005	0.23676	0.08448	0.07897
234 H(1)	0.00097	4.33928	1.54836	1.44743
235 H(1)	-0.00112	-5.02017	-1.79132	-1.67455
236 H(1)	-0.00004	-0.17108	-0.06105	-0.05707
237 H(1)	0.00002	0.09178	0.03275	0.03061
238 H(1)	-0.00006	-0.28847	-0.10293	-0.09622
239 H(1)	-0.00011	-0.47262	-0.16864	-0.15765
240 H(1)	0.00004	0.17663	0.06302	0.05892
241 H(1)	-0.00004	-0.17909	-0.06390	-0.05974
242 H(1)	-0.00004	-0.19375	-0.06914	-0.06463
243 H(1)	0.00007	0.32995	0.11773	0.11006
244 H(1)	-0.00060	-2.68868	-0.95939	-0.89685
245 H(1)	-0.00097	-4.32358	-1.54276	-1.44219
246 H(1)	-0.00000	-0.01271	-0.00453	-0.00424
247 H(1)	-0.00018	-0.81586	-0.29112	-0.27214
248 H(1)	-0.00021	-0.93966	-0.33529	-0.31344
249 H(1)	-0.00007	-0.32174	-0.11481	-0.10732
250 H(1)	-0.00002	-0.07252	-0.02588	-0.02419
251 H(1)	-0.00015	-0.65985	-0.23545	-0.22010
252 H(1)	-0.00001	-0.06425	-0.02292	-0.02143
253 H(1)	-0.00001	-0.02726	-0.00973	-0.00909
254 H(1)	-0.00000	-0.00299	-0.00107	-0.00100
255 H(1)	0.00001	0.02908	0.01038	0.00970
256 H(1)	0.00001	0.03816	0.01362	0.01273
257 H(1)	0.00003	0.14121	0.05039	0.04710
258 H(1)	0.00006	0.27231	0.09717	0.09083
259 H(1)	0.00008	0.37498	0.13380	0.12508
260 H(1)	0.00000	0.02158	0.00770	0.00720
261 H(1)	-0.00003	-0.14423	-0.05147	-0.04811
263 H(1)	-0.00001	-0.03470	-0.01238	-0.01157
264 H(1)	-0.00003	-0.14464	-0.05161	-0.04825

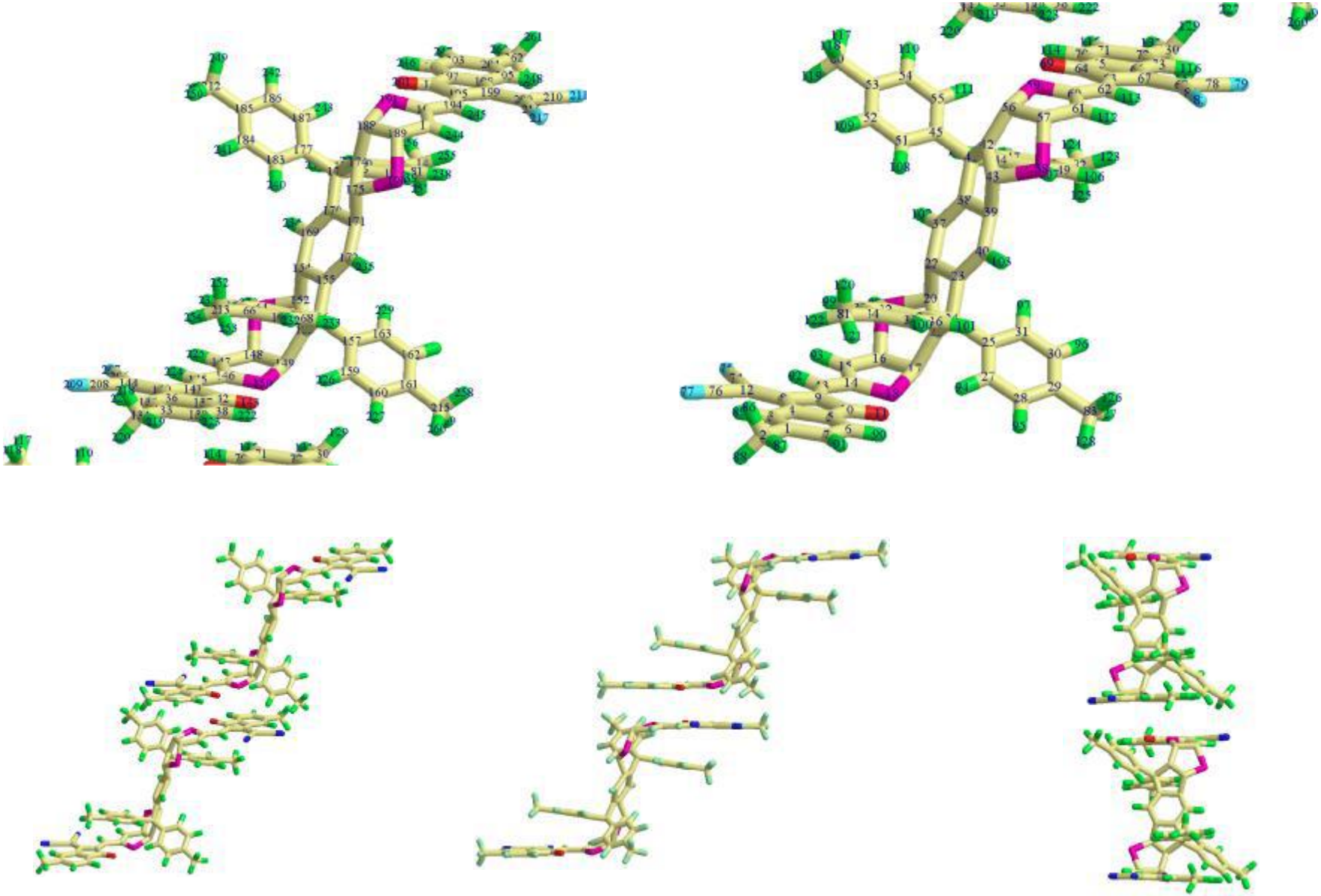

Figure S10. The ^{1}H atoms numbering (above) and different orientations/projections of the 2-ITIC-S-isomer.

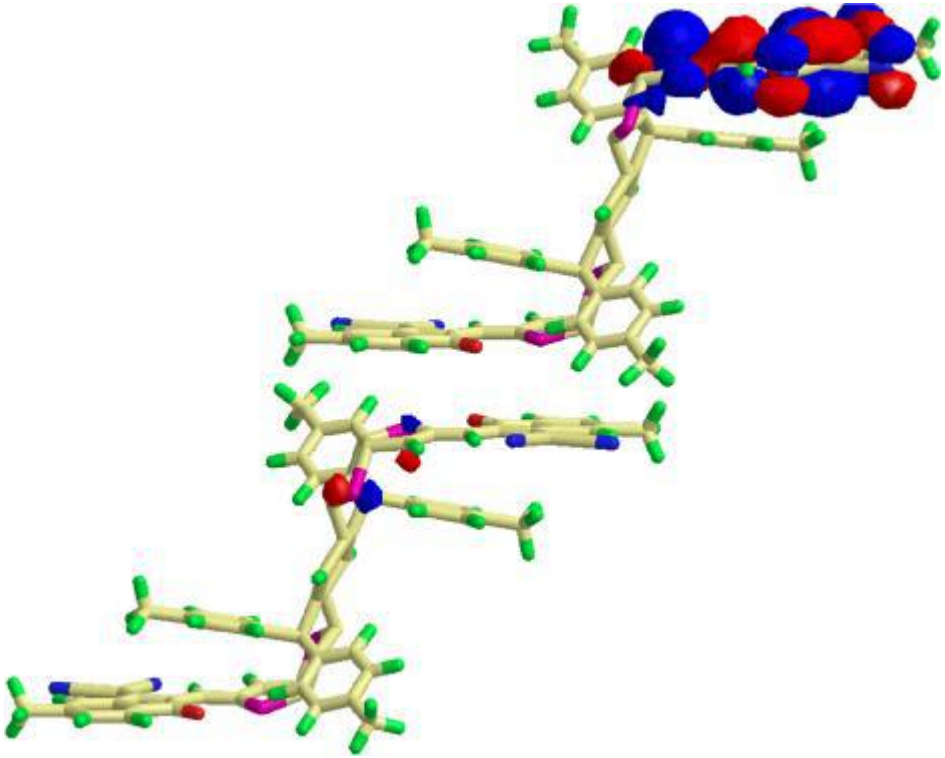

HOMO (-6.194 eV)

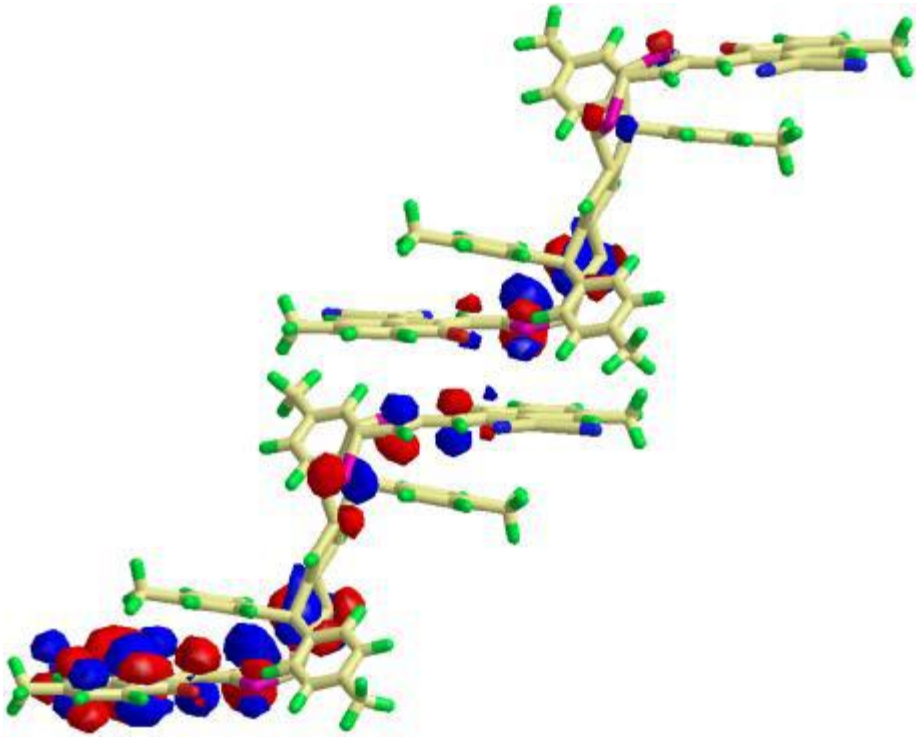

LUMO (-6.117 eV)

Figure S11. HOMO and LUMO energy levels of the 2-ITIC-S-isomer.

SI-VI. Processing of Experimental Spectrum of PBDB-T:ITIC-M Composite

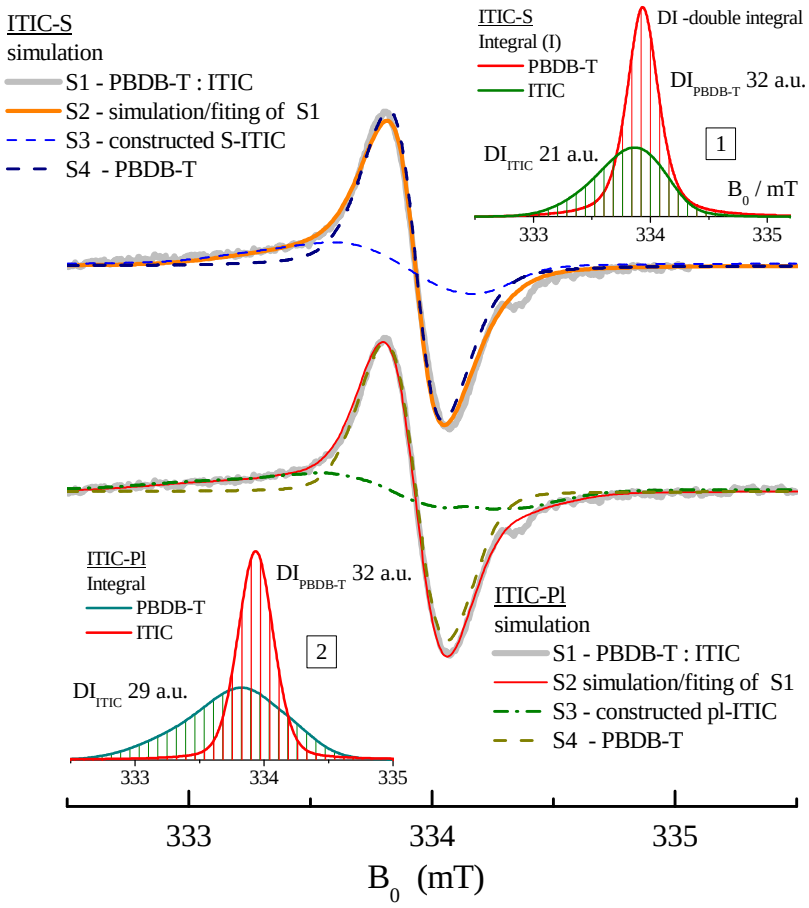

Figure S12. X-band EPR spectrum of PBDB-T:ITIC-M blend film recorded at T = 77 K.

The processing of experimental PBDB-T:ITIC-M LEPR spectra displayed in Fig. S12 indicates a good correlation with ones constructed by DFT for both isomers. However, ITIC-pl demonstrates an excellent result, concerning the conformation of bi-molecular photo-induced process, namely gives equal double integral DI of separated donor/acceptor spectra (see insert 2). In spectra simulation the effective linewidth around 0.2±0.02 mT has been used. Spectral contributions S_3 shown in Fig. S12 are simulated with A_X, A_Y, A_Z summarized in Table S10.

Table S10. Parameters m_i and A_j obtained for ^{1}H of ITIC-pl and ITIC-S configurations.

H_i	m_i	A_X /mT	A_Y/mT	A_Z /mT
		ITIC-pl		
H(85,106)	1/2	-0.6	-0.44	-0.153
H(86,105)	1/2	-0.23	-0.19	-0.7
H(84,108)	1/2	-0.148	-0.125	-0.044
H(82,110)	1/2	-0.148	-0.125	-0.044
ITIC-S				
H(92,113)	1/2	-0.4	-0.29	-0.1
H(93,112)	1/2	-0.155	-0.13	-0.047
H(91,115)	1/2	-0.098	-0.083	-0.03
H(89,116)	1/2	-0.098	-0.083	-0.03

(1) Karlova, G. F.; Umbras, L. P.; Khanin, A. V., Mechanism of Charge Transfer in Gallium Arsenide Light-Emitting Structures. *Russ. Phys. J.* **2003**, *46*, 254-256.

(2) Schubert, E. F., *Light-Emitting Diodes*, 2 ed.; Cambridge University Press: Cambridge, 2012.

(3) Hui, R., *Photo-Electro-Thermal Theory for LED Systems: Basic Theory and Applications*; Cambridge University Press: Cambridge, 2017.

(4) Marumoto, K.; Takeuchi, N.; Ozaki, T.; Kuroda, S., ESR Studies of Photogenerated Polarons in Regioregular Poly(3-Alkylthiophene)-Fullerene Composite. *Synth. Met.* **2002**, *129*, 239-247.

(5) Weil, J. A.; Bolton, J. R.; Wertz, J. E., *Electron Paramagnetic Resonance: Elementary Theory and Practical Applications*; Wiley-Interscience: New York, 2007; Vol. 2d.

(6) Gaussian 16, Revision B.01, M. J. Frisch, G. W. Trucks, H. B. Schlegel, G. E. Scuseria, M. A. Robb, J. R. Cheeseman, G. Scalmani, V. Barone, G. A. Petersson, H. Nakatsuji, X. Li, M. Caricato, A. V. Marenich, J. Bloino, B. G. Janesko, R. Gomperts, B. Mennucci, H. P. Hratchian, J. V. Ortiz, A. F. Izmaylov, J. L. Sonnenberg, D. Williams-Young, F. Ding, F. Lipparini, F. Egidi, J. Goings, B. Peng, A. Petrone, T. Henderson, D. Ranasinghe, V. G. Zakrzewski, J. Gao, N. Rega, G. Zheng, W. Liang, M. Hada, M. Ehara, K. Toyota, R. Fukuda, J. Hasegawa, M. Ishida, T. Nakajima, Y. Honda, O. Kitao, H. Nakai, T. Vreven, K. Throssell, J. A. Montgomery, Jr., J. E. Peralta, F. Ogliaro, M. J. Bearpark, J. J. Heyd, E. N. Brothers, K. N. Kudin, V. N. Staroverov, T. A. Keith, R. Kobayashi, J. Normand, K. Raghavachari, A. P. Rendell, J. C. Burant, S. S. Iyengar, J. Tomasi, M. Cossi, J. M. Millam, M. Klene, C. Adamo, R. Cammi, J. W. Ochterski, R. L. Martin, K. Morokuma, O. Farkas, J. B. Foresman, and D. J. Fox, Gaussian, Inc., Wallingford CT, 2016.